

Article

Ocean Impacts on Australian Interannual to Decadal Precipitation Variability

Zachary F. Johnson ^{1,*}, Yoshimitsu Chikamoto ¹, Jing-Jia Luo ² and Takashi Mochizuki ³

¹ Department of Plants, Soils and Climate, Utah State University, Logan, UT 84341, USA; yoshi.chikamoto@usu.edu

² Bureau of Meteorology, Melbourne, VIC 3008, Australia; jing-jia.luo@bom.gov.au

³ Japan Agency for Marine-Earth Science and Technology (JAMSTEC), Yokohama 236-0001, Japan; motizuki@jamstec.go.jp

* Correspondence: zjohnson@aggiemail.usu.edu; Tel.: +1-435-797-2233

Received: 31 May 2018; Accepted: 9 July 2018; Published: 11 July 2018



Abstract: In Australia, successful seasonal predictions of wet and dry conditions are achieved by utilizing the remote impact of sea surface temperature (SST) variability in tropical oceans, particularly the Pacific Ocean, on the seasonal timescale. Beyond seasonal timescales, however, it is still unclear which processes and oceans contribute to interannual-to-decadal wet/dry conditions in Australia. This research examines the interannual-to-decadal relationship between global SST anomalies (SSTAs) and Australian wet/dry variability by analyzing observational data and global climate model experiments conducted with the NCAR Community Earth System Model (CESM) and the Model for Interdisciplinary Research on Climate (MIROC). A 10-member ensemble simulation suite for 1960–2015 (CESM) and 1950–2010 (MIROC) is conducted by assimilating the observed three-dimensional ocean temperature and salinity anomalies into fully coupled global climate models. In both observational analyses and ocean assimilation experiments, the most dominant annual mean precipitation variability shows a clear relationship with SSTAs in the tropical Pacific and the Atlantic. Our partial ocean assimilation experiment, in which the ocean component of the CESM and MIROC are assimilated by the observed ocean temperature and salinity anomalies in the equatorial Pacific only, shows that the tropical Pacific SST variability is the main driver of Australian precipitation variability on the interannual-to-decadal timescales. However, our additional partial ocean assimilation experiment, in which the climate models incorporate the observed anomalies solely in the Atlantic ocean, demonstrates that the Atlantic Ocean can also affect Australian precipitation variability on the interannual-to-decadal timescale through changes in tropical Pacific SSTAs and the modulation of the global Walker circulation. Our results suggest that about a half of Australian interannual-to-decadal precipitation variability originates from the Atlantic Ocean.

Keywords: Australia; precipitation; drought; decadal variability; climate model; ENSO; TBV

1. Introduction

Australia experiences prolonged or intermittent severe droughts that devastate local economies, put significant strain on the agriculture industry and contribute to wildfires [1,2]. For example, the Millennium Drought (1997–2010) impacted the populated areas of Australia, including cities like Melbourne, Brisbane, and Sydney causing severe water restrictions and a ban on outdoor water use [3]. In addition, a significant drop in the gross domestic product was observed and blamed on the drought in Australia [4]. Conversely, Australia is susceptible to flooding, which affects major metropolitan areas, for example, the 1976 Brisbane and 2002 Townsville floods [5,6]. Due to Australia

being surrounded by oceans on all sides, many studies have looked into the ocean's impact on climate extremes in Australia, as introduced below.

The El Niño Southern Oscillation (ENSO) interactions between large-scale sea surface temperature (SST) anomalies (SSTAs) and atmospheric circulation have a significant impact on drought conditions around the world, including Australia [7]. ENSO is split into three categories: La Niña or cooling of the equatorial Pacific, neutral or a lack of temperature anomalies in the equatorial Pacific, and El Niño or warming of the equatorial Pacific. Previous studies have shown the linkage of El Niño to some of the major droughts in Australia [2,8–11]. Through tightly coupled atmosphere–ocean interactions, ENSO accompanies a zonal see-saw of atmospheric pressure anomalies in the Australian–Indonesian and Eastern equatorial Pacific regions, which is known as Walker Circulation [12]. As a result, many studies have shown ENSO to affect a significant portion of Australian precipitation variability. We note that some of Australian precipitation events could be explained by the other drivers outside the tropical Pacific [13]. Because of the predictability of ENSO (in the order of one or two years), climatologists and meteorologists apply ENSO prediction to their seasonal climate forecasts [14,15]. Additionally, the Indian Ocean Dipole (IOD) can also affect the precipitation variability over Australia and potentially cause decadal predictability [16–18]. It would be of great benefit for society if we could enhance the predictability of Australian precipitation anomalies and lead times beyond seasonal timescales.

While the Walker Circulation is mainly located within the Pacific region in the traditional sense of the term, similar atmospheric asymmetric zonal circulations are also observed in other ocean basins, such as the equatorial Indian Ocean and Atlantic regions [16,19]. It is known that, on interannual timescales, the three tropical oceans display intimate interactions that affect the IOD, ENSO, and Atlantic Niño [20,21]. On decadal timescales, recent studies have also suggested that the tropical Pacific interacts with the Indian and Atlantic Oceans through the modulation of global Walker circulation despite being separated by continents [22–27]. Additionally, the Indian ocean can influence the Pacific Ocean through the atmospheric bridge [23,28]. This leads to the inter-basin scale decadal climate variability. Some state-of-the-art climate prediction systems have demonstrated that the tropical inter-basin interaction between the Pacific, Atlantic, and Indian Oceans shows multi-year predictive skills [21,29,30]. Moreover, there is evidence that oceans can provide decadal predictability in Australia given the ocean's large effect on the continent [31]. Nevertheless, it is still unclear whether and how tropical oceans affect the precipitation variability at interannual-to-decadal timescales in Australia.

In this study, we examine Australian the interannual-to-decadal precipitation variability originating from the ocean using two global climate models: the Community Earth System Model (CESM) and the Model for Interdisciplinary Research on Climate (MIROC). In these models, observed three-dimensional ocean temperature and salinity anomalies are assimilated and external radiative forcings are prescribed. By identifying the consistent variability between observations and model simulations, we discuss how the tropical Pacific and Atlantic Oceans contribute to Australian precipitation variability. We note that possible contributions of the Indian Ocean are not examined in the work considering the relatively small impact of the Indian Ocean on Pacific decadal change in recent decades [29]; however, the potential role of the Indian Ocean is discussed in Section 4.

2. Data and Model Experiments

2.1. Observational Datasets

Our model experiments are validated by observational datasets including precipitation from the Global Precipitation Climatology Centre (GPCC), monthly mean sea level pressure (SLP) derived from the National Centers for Environmental Prediction (NCEP) reanalysis, and sea surface temperature (SST) from the Extended Reconstructed Sea Surface Temperature version 4 (ERSSTv4). Precipitation from the GPCC is based off over 67,000 stations worldwide and has a grid spacing of 0.5° , ranging from

1901–2016 [32]. SLP extends from 1948–2015 with a 2.5° resolution [33]. SST has a 2° resolution extending from 1854–2016 [34]. These reconstructed datasets use statistical analyses for spatial completeness, especially since observations from earlier years are more sparse.

2.2. Models

This study used two fully-coupled, low-resolution models: the CESM 1.0.3 [35] and the MIROC 3.2 m [36]. The CESM relies on physics data from the Community Climate System Model [37] version 4, which includes atmospheric dynamics from the Community Atmosphere Model [38] version 4. The resolutions for atmospheric and land are T31 spectral (approximately 3.75°) including hybrid sigma pressure coordinates of 26 atmospheric levels and 15 soil levels (surface: 35 m). The ocean model includes 60 vertical levels and is coupled with the sea-ice model, which has a resolution of approximately 3°. Within the CESM, the land, atmosphere, and sea-ice communicate every 30 min, while the ocean couples with the atmosphere once a day. The land portion is from the Community Land Model version 4 and has a carbon–nitrogen biogeochemical cycle, a groundwater model, and a wildfire scheme [39]. Details of the model's basic performance in the configuration can be found in the results of the CESM described in previous studies [35,40].

The MIROC uses a T42 spectral horizontal grid, including 20 vertical levels of sigma pressure coordinates and a standard physics package cooperatively developed at the Center for Climate System Research (CCSR), the University of Tokyo's Atmosphere and Ocean Research Institute, and the Frontier Research Center for Global Change [41]. The ocean component has a higher resolution (1.4°-latitude and 0.56–1.4°-longitude) compared to the CESM with 44 levels. All components of atmosphere, ocean, land, and sea-ice modules are coupled without any flux corrections for exchanging heat, water, and momentum fluxes between the atmosphere and the ocean. [42]. Details of the performance and settings of the MIROC were described in a previous study [36].

2.3. Partial Assimilation Experiments

In this study, we analyzed ocean data assimilation experiments as described in previous studies [40,43–45]. Both the CESM and MIROC runs consisted of 10 ensemble members with time-varying observed external forcings (solar, aerosols, land-use change, and greenhouse gases) prior to 2005. After 2005, we prescribed the RCP4.5 emission scenario for the CESM and the A1B-type scenario for the MIROC. Using these configurations for the external forcings, the observed global three-dimensional ocean temperature and salinity anomalies (CESM: 0–3000 m; MIROC: 0–700 m) were assimilated into the ocean components of global climate models (the global ocean assimilation runs). By assimilating the surface and sub-surface ocean fields, the models were able to simulate the ocean variability in the mixed layer depth, thermocline, and thermodynamics more appropriately compared to an SST-only assimilation. As a result, our assimilation run was suitable for the investigation of the interannual-to-decadal climate variability. The observations were derived from the ECMWF ocean reanalysis product (version 4) for 1958–2014 in the CESM, but the objective analysis was termed ProjD for 1945–2010 in the MIROC [46,47]. The monthly observations of these datasets were linearly interpolated into daily values and then assimilated into the ocean model component in each climate model using an Incremental Analysis Update scheme [48,49]. The ocean assimilation systems were developed individually in each model, but they were applied using a similar method. More detailed methodology and its application for decadal climate prediction have been described by previous studies of the MIROC [50,51] and the CESM [52].

To evaluate the ocean contribution to Australian precipitation, we partially assimilated the observed three-dimensional ocean temperature and salinity anomalies in the equatorial Pacific (CESM and MIROC: 10° S–10° N) and the entire Atlantic (CESM: 30° S–70° N; MIROC: 50° S–60° N), respectively. Each partial assimilation and global runs included 10 ensemble members with different time ranges for the CESM (1960–2014) and MIROC (1950–2010) after the model spin-up (2 years for the CESM and 5 years for the MIROC). The ensemble mean was used to analyse the data. The initial

conditions for the assimilation runs were obtained from 10-member initial conditions within the twentieth century historical simulation as designed by the Coupled Model Intercomparison Project-5 (i.e., prescribing the observed external forcings without ocean data assimilation). Our assimilation procedure took into account the model climatological biases and had no significant model drift in the global and partial ocean data assimilation runs. These assimilation systems were developed in order to conduct decadal climate predictions in previous studies [50,52]. The partial assimilation experiments captured both the low frequency atmospheric response to SST variability in the partially assimilated area (i.e., Atlantic or equatorial Pacific) and air–sea interaction responses that are remotely forced by the partially assimilated ocean. Partial assimilation and similar experiments were conducted in previous studies [25–27,29,44,53,54] and the use of two separate general circulation models allowed us to evaluate the robust features as well as the model uncertainty.

3. Results

3.1. Model Validation

To capture the most correlated variability of Australian precipitation between observations and model simulations, we conducted a singular value decomposition (SVD) analysis [55] (similar to the maximum covariance analysis but using a correlation matrix) from the annual mean precipitation anomalies over Australia (45° S–10° S, 105° E–160° E) between the GPCP and the ensemble mean of the model global runs (top panels in Figures 1 and 2). Because of the different lengths of the model simulations, the SVD analysis was applied from 1960–2014 in the CESM and from 1950–2010 in the MIROC. Nevertheless, the first SVD mode in both the CESM and MIROC versus the observations explained most of the variance of the Australian precipitation variability through the square covariance fraction (SCF), the percentage of square covariance between the two fields explained in the leading SVD mode (SCF = 85.5% and 88.6%, respectively). The model's simulated temporal variations in the first SVD mode were highly correlated with the observed variations (correlation coefficient $R = 0.66$ in the CESM and 0.65 in the MIROC; Figures 1c and 2c). The observed precipitation pattern associated with the first SVD mode showed a monopole structure for the entirety of Australia with a local maximum on the Eastern side (Figures 1a and 2a). This monopole pattern was also captured by the first SVD mode of global runs in both the CESM and MIROC very well (Figures 1b and 2b), although both models overestimated the precipitation anomalies over Western Australia. In particular, the first SVD mode captured the multi-year wet periods around the mid-1970s and late-1990s and additionally, the dry periods around the early-1990s and early-2000s (Figures 1c and 2c). During these periods, Australia experienced severe flooding events in Brisbane [6] in 1974, Townsville [5] in 1998, and in Queensland [56] in 2010–2011, and also, a drought occurred in Queensland [57] in the early-1990s as well as the millennium drought [2] in the early-2000s. In fact, the observed and model-simulated principal components of these first SVD modes (black and red lines in Figures 1c and 2c) exhibited a larger power in the lower frequency components with a spectral peak at 12.5 years (a frequency of 0.08 cycles per year) in both the CESM and MIROC (black lines in Figure 3). Our SVD analysis suggests that these wet and dry conditions are mainly attributed to the SSTAs in Australian precipitation variability.

Figures 4a and 5a show the observed patterns of SST and SLP anomalies associated with the first SVD mode between the GPCP observation and the global assimilation runs. We found La Niña-like SST and SLP anomaly patterns which were characterized by SST cooling in the central tropical Pacific, its surrounding warming in the Western Pacific, and a zonal pressure gradient with positive SLP anomalies in the Eastern tropical Pacific and negative ones in the Indo-Western Pacific regions. This zonal SLP gradient associated with the first SVD mode corresponded to the strengthened (weakened) Walker circulation in the Indo-Pacific sector during enhanced (suppressed) Australian precipitation years. The La Niña-like patterns accompanied the warm SSTAs around the Australian coastline and the lower-than-normal SLP covering its entire continent, which is consistent with the

increase in Australian annual precipitation. These features were captured very well in the global runs of both the CESM and MIROC (Figures 4b and 5b), indicating that the SSTAs play an important role in the Australian interannual-to-decadal precipitation variability. These results suggest that our model experiments are a reasonable method to evaluate the ocean impacts on the Australian precipitation variability.

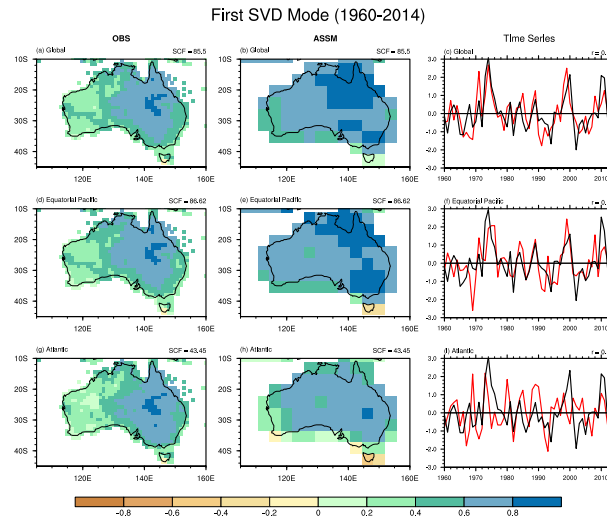


Figure 1. The first singular value decomposition (SVD) modes of annual mean precipitation anomalies in Australia between observations (Global Precipitation Climatology Centre; GPCC) and the Community Earth System Model (CESM) simulations of the (a–c) global assimilation run and the partial assimilation runs in the (d–f) equatorial Pacific and the (g–i) Atlantic during 1960–2014. The left and middle columns are homogeneous correlation maps in the observation and model simulations, respectively. The squared covariance fraction (SCF) explained by the first SVD mode is indicated in the upper-right corner of these panels. The right column shows the principal components of the first SVD modes between observations (black) and model simulations (red). Correlation coefficients of these principal components in the first SVD mode are noted in the top right of each time series plot. The correlation coefficient of 0.35 was statistically significant at the 99% level with 50 degrees of freedom. The SVD analysis was conducted based on the correlation matrix.

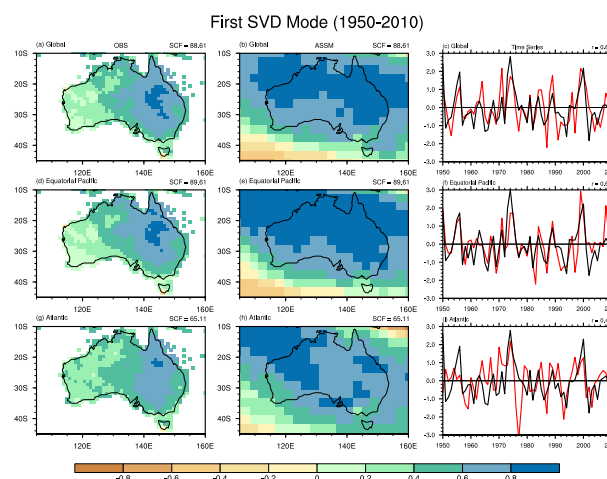


Figure 2. The first SVD modes of annual mean precipitation anomalies in Australia between observations (GPCC) and the Model for Interdisciplinary Research on Climate (MIROC) simulations of the (a–c) global assimilation run and the partial assimilation runs in the (d–f) equatorial Pacific and the (g–i) Atlantic during 1950–2010, which is the same as Figure 1 but for the MIROC.

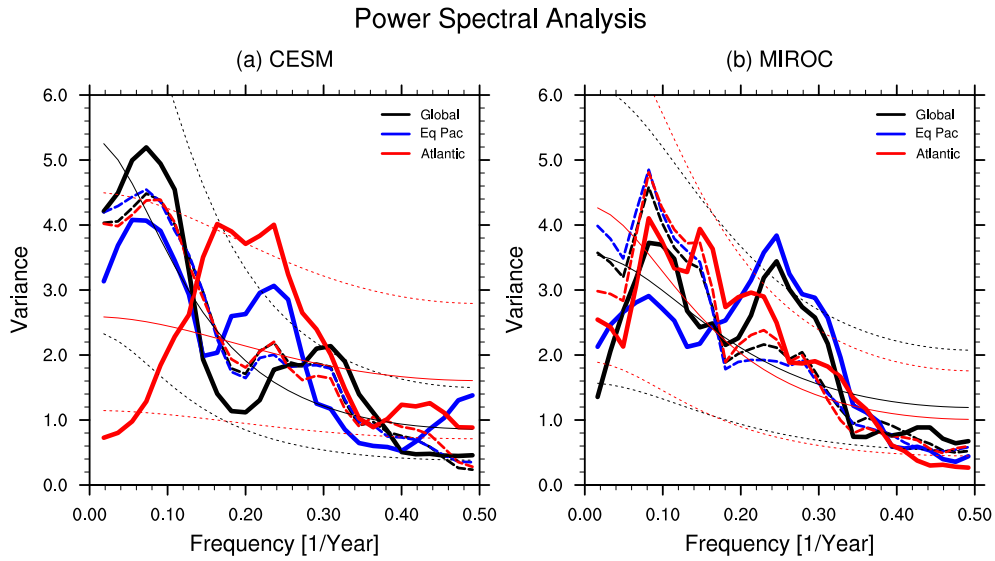


Figure 3. Power spectrum for the principal components of the first SVD mode in observations (broken lines) and model simulations (thick solid lines) in the global (black), equatorial Pacific (blue), and Atlantic (red) assimilation runs in the (a) CESM and the (b) MIROC. The thin solid line and thin dotted line correspond to the power spectrum of a fitted first order Markov process and its 95% and 5% confidence limits for model simulations in the Atlantic (red) and global (black) runs, respectively.

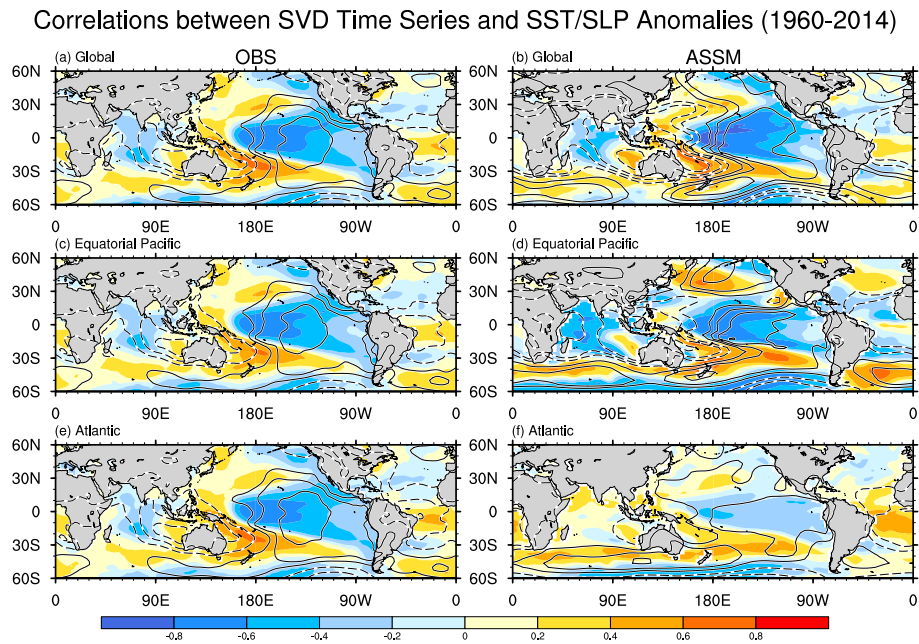


Figure 4. Correlation maps of sea surface temperature (SST) (shade) and sea level pressure (SLP) anomalies (contour: solid and broken lines are positive and negative correlations, respectively) associated with the first SVD mode between the (left) observations and the (right) CESM simulation in the (a,b) global, (c,d) equatorial Pacific, and (e,f) Atlantic assimilation runs during 1960–2014. The contour interval is 0.2 and the zero contour is omitted. The observed SST and SLP datasets were obtained from the Extended Reconstructed Sea Surface Temperature (ERSST) and the National Centers for Environmental Prediction (NCEP), respectively.

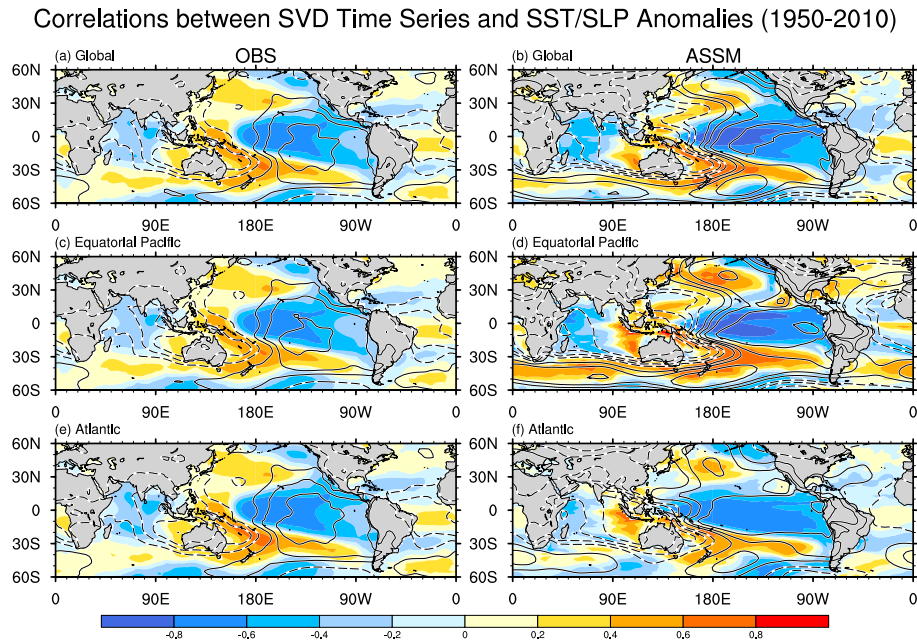


Figure 5. Correlation maps of sea surface temperature (SST) (shade) and sea level pressure (SLP) anomalies (contour: solid and broken lines are positive and negative correlations, respectively) associated with the first SVD mode between the (left) observations and the (right) MIROC simulation in the (a,b) global, (c,d) equatorial Pacific, and (e,f) Atlantic assimilation runs during 1950–2010. This figure is the same as Figure 4 but for the MIROC.

3.2. Ocean Impacts on Australian Precipitation Variability

As described in the previous subsection, the first SVD modes of Australian precipitation between the observations and global runs of both the CESM and MIROC accompanied significant SST correlations in the equatorial Pacific with a wide swath exceeding -0.6 (Figures 4b and 5b), suggesting that the equatorial Pacific SST is the primary driver for Australian precipitation variability. To further explore this, we applied an SVD analysis for the Australian precipitation variability between the observations and ensemble means of the equatorial Pacific partial assimilation runs (Figures 1d,f and 2d,f). Similar to the results in the global runs, the first SVD mode between the observations and the equatorial Pacific runs explained most of the variance in both the CESM and MIROC (86.6% and 89.1%). These first SVD modes showed significant correlation coefficients of principal components between the observations and model simulations in both the CESM and MIROC ($R = 0.63$ and 0.67 in Figures 1f and 2f) and exhibited monopole precipitation patterns over Australia (Figures 1c,d and 2c,d) that were almost identical to the results of the global runs (Figures 1a,b and 2a,b). These first SVD modes of Australian precipitation variability in the equatorial Pacific partial assimilation runs demonstrated the La Niña-like pattern, including the central tropical Pacific SST cooling and the positive zonal gradient of SLP anomalies between the Eastern tropical Pacific and the Indo-Western Pacific region (Figures 4d and 5d). This result strengthens the suggestion that the La Niña-like SST forcing in the equatorial Pacific is the main driver of the enhanced annual precipitation in Australia and vice versa. We can see the lower-than-normal SLP anomalies over the entire Australian continent were associated with the weakened Pacific Walker circulation (Figures 4d and 5d), which is consistent with the enhanced precipitation over Australia (Figures 1e,f and 2e,f). There were also significant correlations in the model-simulated principal components of the first SVD modes between the global runs and the equatorial Pacific partial assimilation runs for both the CESM (red lines in Figure 1c,f; $R = 0.71$) and the MIROC (red lines in Figure 2c,f; $R = 0.79$), further strengthening this result. Although ENSO is a major driver of Australian precipitation variability on seasonal

timescales [7], a similar mechanism showing the equatorial Pacific Ocean impacts on the Australian precipitation was found even on the decadal timescale (Figure 3).

There is evidence that the Atlantic ocean may affect the tropical Pacific climate variability [25–27,29], and, in turn, potentially affect Australian precipitation [30]. To identify the Atlantic origin of Australian precipitation variability, we applied the SVD analysis to the Australian precipitation variability between the observations and ensemble means of the Atlantic partial assimilation runs (Figures 1g–i and 2g–i). The first SVD modes in the Atlantic partial assimilation runs explained 43.5% in the CESM and 65.1% in the MIROC for total covariance, which were well separated from higher modes (the SCFs of second SVD modes in the CESM and MIROC are 17% and 11.1%, respectively). The correlation coefficients of the principal components in the leading SVD modes were statistically significant ($R = 0.37$ in the CESM and 0.46 in the MIROC). The Atlantic partial assimilated experiment also captured a very similar positive monopole-like pattern for the observed precipitation variability that was comparable to the global and equatorial Pacific runs (Figures 1 and 2). The observed principal components of the first SVD modes in the global, equatorial Pacific, and Atlantic runs were almost identical to each other (black lines in Figures 1c,f,i and 2c,f,i; $R > 0.95$). In addition to the Australian precipitation variability, the observed SST and SLP anomalies correlated with these first SVD modes and also showed indistinguishable patterns from each other (left panels in Figures 4 and 5). Even though the model-simulated precipitation variability is driven by the different ocean basins, the SVD analysis captured the same observed precipitation variability in Australia.

In the Atlantic partial assimilation runs, the first SVD mode accompanied the equatorial Pacific SST cooling (Figures 4f and 5f) and the enhanced precipitation over Australia (Figures 1h and 2h), similarly to the results of the global and equatorial Pacific runs. Previous studies have indicated that the Atlantic Ocean variability can drive the tropical Pacific climate variability through modulation of the global Walker circulation [25–27,29]. Consistent with these results, our Atlantic partial assimilation run demonstrates that the SST cooling in the equatorial Pacific partially originates from the Atlantic Ocean variability, which further enhances precipitation in Australia. This negative correlation between the Eastern equatorial Pacific SST and Australian precipitation in the Atlantic partial assimilation run was stronger in the MIROC than in the CESM (Figures 4f and 5f). In fact, the first SVD mode in the MIROC Atlantic partial assimilation runs clearly showed equatorial Pacific SST cooling and lower-than-normal SLP over the Australian continent (Figure 5f) though those responses were much weaker in the CESM Atlantic partial assimilation run (Figure 4f). In any case, our results suggest that the Atlantic is able to trigger the central Pacific SST variability and the subsequent changes in Australian annual precipitation.

3.3. Atlantic Origin Changes in Australian Precipitation

To identify the Atlantic origin of the central tropical Pacific SST variability, we produced a scatter plot of the annual mean SSTAs in the Niño 4 region (5°S – 5°N , 160°E – 150°W) between the observations and the Atlantic partial assimilation runs of the CESM and MIROC (Figures 6 and 7). Similar results were obtained when we use the global assimilation runs instead of the observations. The Niño 4 region was chosen over the Niño 3.4 region (5°S – 5°N , 170°E – 120°W) because it has a lower frequency [58,59]. The points at the upper-right and lower-left quadrants imply that the SSTAs in the central tropical Pacific originate from the Atlantic Ocean variability, whereas those at the upper-left and lower-right quadrants indicate the lesser role of the Atlantic Ocean in causing the tropical Pacific SST variability. By choosing the consistent years in the central tropical Pacific SSTAs between the observations and the Atlantic partial assimilation runs, we evaluated the Atlantic impacts on the Australian precipitation variability via changes in the tropical Pacific climate. For the CESM, we found eight cold years in the central tropical Pacific SSTAs associated with the Atlantic forcing (below -0.5°C ; 1964, 1984, 1988, 1989, 1998, 1999, 2010 and 2011) but only three warm years (above 0.5°C ; 1977, 2004 and 2009). A higher number of years was extracted in the MIROC Atlantic partial assimilation run: 10 cold years (1964, 1971, 1973, 1974, 1984, 1985, 1988, 1989, 1999 and 2000) and nine warm years (1957,

1958, 1977, 1987, 1993, 2002, 2003, 2004 and 2005). Clearly, the MIROC (Figure 6) was able to produce more warm and cold years compared to the CESM (Figure 7), which enhanced the correlation for the MIROC ($R = 0.29$) compared to the CESM ($R = 0.00$). This higher correlation in the MIROC compared to the CESM is consistent with the SVD analysis in the Atlantic partial assimilation run, in which the central tropical Pacific SST cooling was much larger in the MIROC than the CESM (Figures 4f and 5f).

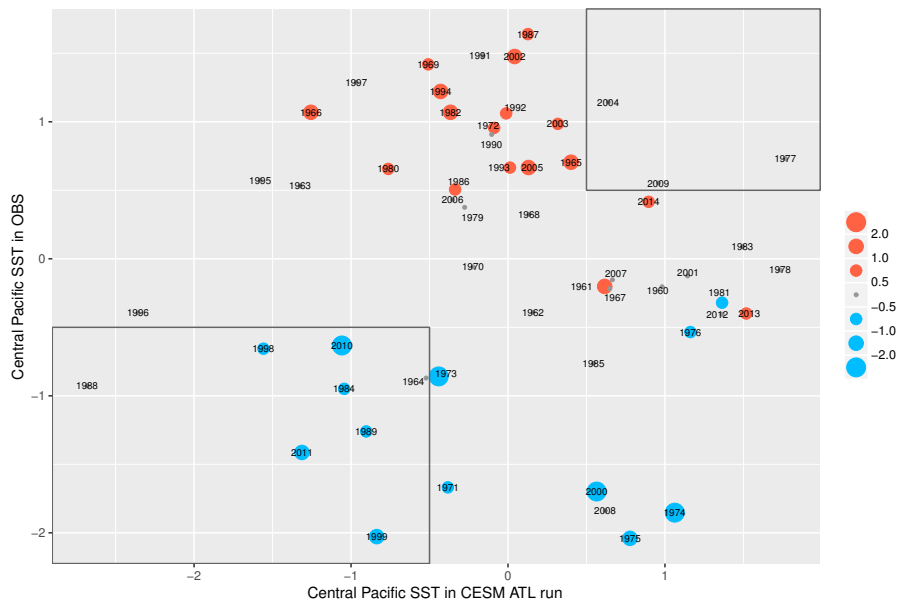


Figure 6. Scatterplot of large-scale SST anomalies (SSTAs) averaged over the Niño 4 region in observation and the CESM Atlantic partial assimilation run from 1960–2014. The Niño 4 values were standardized with the standard deviation of the dataset. Composite years were chosen for those exceeding or being less than 0.5 and -0.5 standard deviations for both the observations and the Atlantic partial assimilation runs (black box). The dot size and color indicate the observed principal components in the SVD analysis between the observation and the Atlantic partial assimilation runs (black line in Figure 1i). $R = 0.00$.

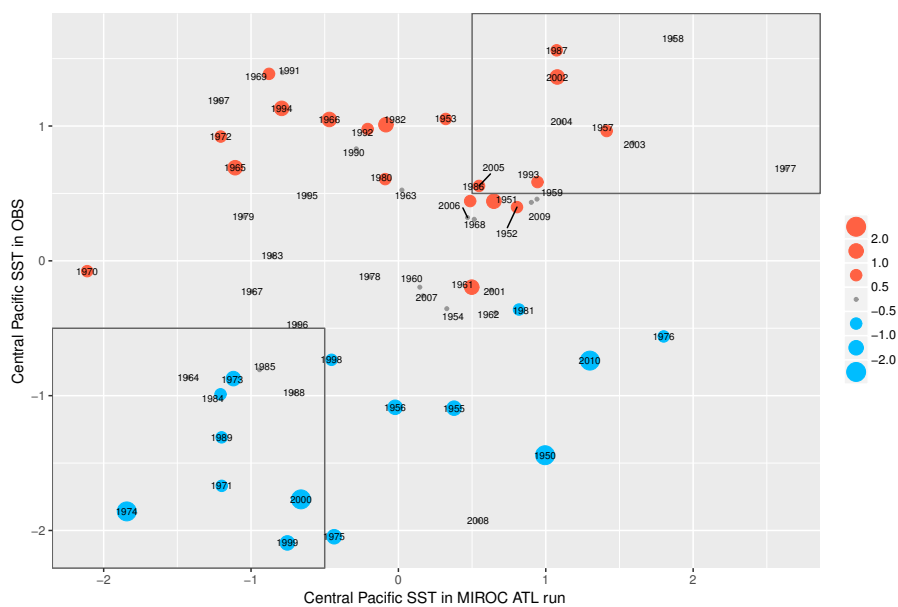


Figure 7. Same as Figure 6 but for the MIROC during 1950–2010. $R = 0.29$.

Using the cold and warm years extracted from the scatter plots of the central tropical Pacific SSTAs (Figures 6 and 7), we conducted a composite analysis of annual precipitation anomalies in Australia (Figures 8 and 9). Consistent with the SVD analysis, the observed annual precipitation anomalies tended to show wet conditions for the entirety of Australia during cold years, but dry conditions were observed during warm years (left panels in Figures 8 and 9). During cold years, in particular, the enhanced precipitation anomalies in Eastern Australia were well simulated in the equatorial Pacific and the Atlantic partial assimilation runs of both the CESM and MIROC (Figure 8). We can also confirm the consistency with the SVD analysis, whereby those cold years showed larger observational principal components in the first SVD mode (blue dots in Figures 6 and 7), except for 1964, 1985, and 1988. Similar features, but in an opposite phase, were also obtained in the warm year composite in the MIROC (bottom panels in Figure 9), though the warm year composite in the CESM showed a noisier pattern because of the smaller sampling number of warm years (only three years; upper panels in Figure 9). Additionally, in the warm composite years, precipitation anomalies in the CESM Atlantic run showed almost no statistical significance over Australia (black dots in Figure 9c). Because of this lesser Atlantic impact on the warmer SSTAs in the central tropical Pacific, the Atlantic partial assimilation run in the CESM, compared to the MIROC, showed a weaker impact on Australian precipitation variability.

Cold Year Composite Analysis

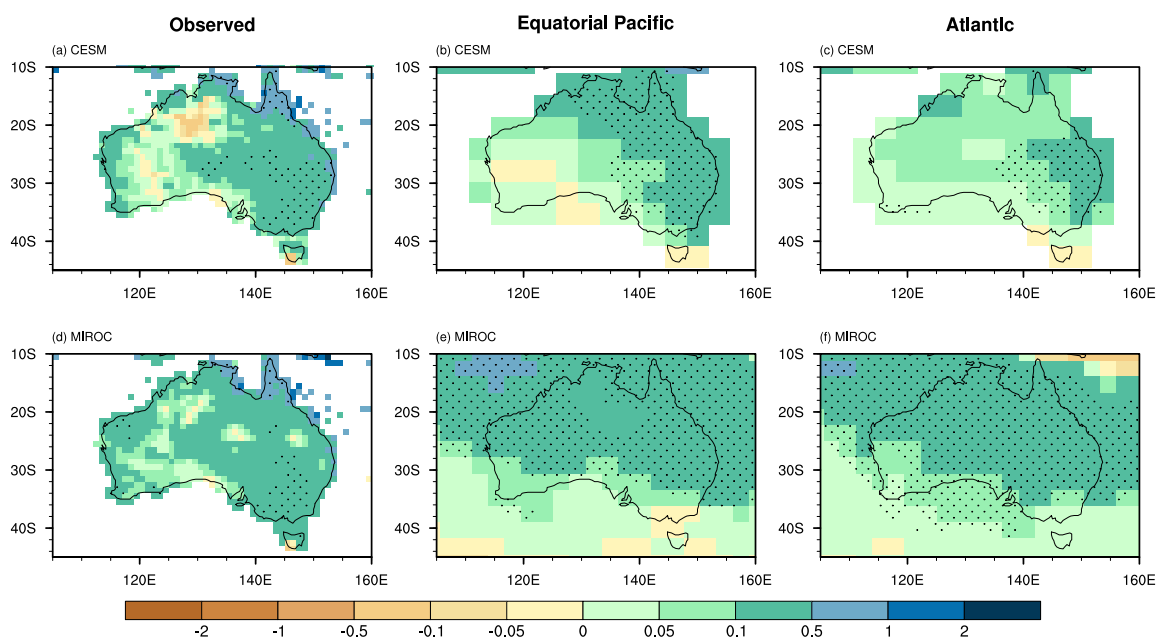


Figure 8. Annual precipitation anomalies (mm/day) in (a,d) observation, the (b,e) equatorial Pacific, and the (c,f) Atlantic partial assimilation runs during the cold year composites in the (top) CESM and the (bottom) MIROC. The dotted region is above the 90% statistical significance level using Student's *t*-test for precipitation anomalies. The cold years are obtained from scatter plots in Figures 6 and 7, in which the annual SSTAs in the Niño 4 region are below -0.5 standard deviations in both observation and the Atlantic partial assimilation runs of the CESM (1964, 1984, 1988, 1989, 1998, 1999, 2010 and 2011) and the MIROC (1964, 1971, 1973, 1974, 1984, 1985, 1988, 1989, 1999 and 2000).

Figures 10 and 11 show the SST and SLP anomaly patterns in the cold and warm year composites. For the cold composite years, in both the CESM and MIROC, the observations showed equatorial Pacific SST cooling and the zonal SLP anomaly gradient in the tropical Pacific with the dominant negative SLP anomalies over Australia and the Eastern Indian Ocean (left panels in Figure 11). These SST and SLP anomaly patterns were captured well in the equatorial Pacific partial assimilation runs in both

the CESM and MIROC models (middle panels in Figure 11), indicating that the equatorial Pacific SST cooling and subsequent Australian decreased SLP anomalies were the main factors in the enhanced precipitation in Australia. The Atlantic partial assimilation runs in both the CESM and MIROC also captured these features, albeit with almost half of the amplitudes of the equatorial Pacific SST cooling compared to the observations and the equatorial Pacific partial assimilation runs (right panels in Figure 11). Similar features, but opposite phases, were obtained for the warm year composite in the MIROC (bottom panels in Figure 10). These results strongly support the finding that the Atlantic Ocean variability contributes to the Australian precipitation variability through changes in SLP anomalies over the Australian continent via the equatorial Pacific SST forcing.

Warm Year Composite Analysis

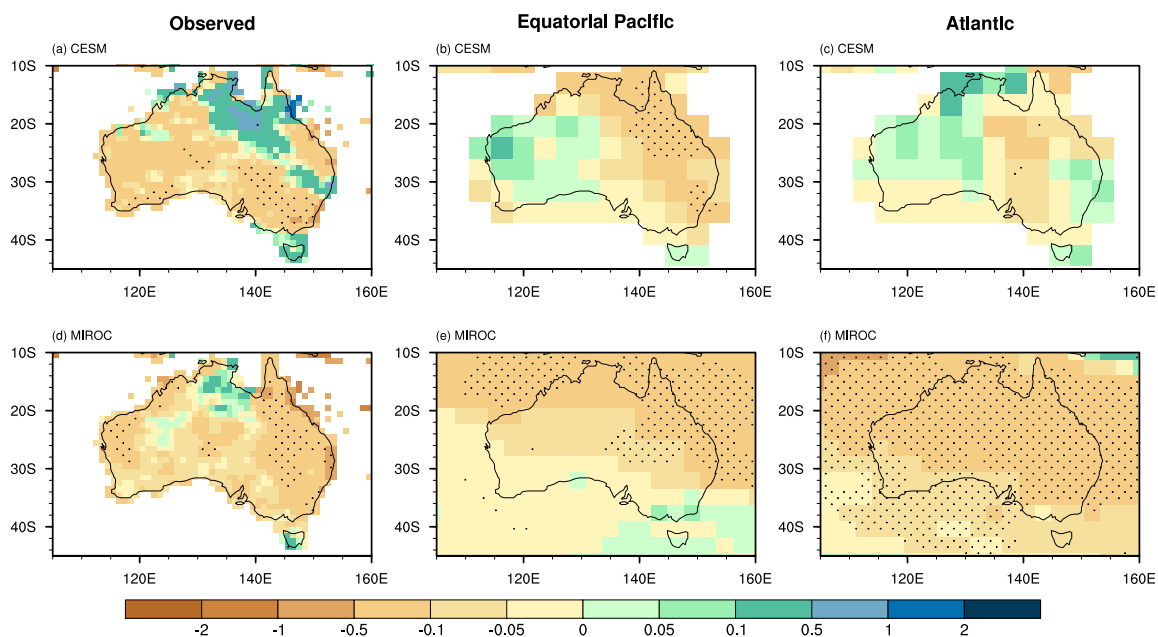


Figure 9. Annual precipitation anomalies (mm/day) in (a,d) observation, the (b,e) equatorial Pacific, and the (c,f) Atlantic partial assimilation runs during the warm year composites in the (top) CESM and the (bottom) MIROC. This figure is the same as Figure 8 but for the warm year composite. The dotted region is above the 90% statistical significance level using Student's *t*-test for precipitation anomalies. The cold years are obtained from scatter plots in Figures 6 and 7, in which the annual SSTAs in the Niño 4 region are above -0.5 standard deviations in both observation and the Atlantic partial assimilation runs CESM (1977, 2004, and 2009) and the MIROC (1957, 1958, 1977, 1987, 1993, 2002, 2003, 2004, and 2005).

On the other hand, the warm year composite in the CESM may have a different process in terms of Atlantic impacts on Australian precipitation variability. The CESM warm year composite shows the northwest–southeast SLP anomaly gradient over the Australian continent in all of the observations, the equatorial Pacific, and the Atlantic partial assimilation runs even though there are warmer SSTAs in the equatorial Pacific (upper panels in Figure 10). Because of the geostrophic balance, this SLP gradient within the Australian continent accompanies the southerly wind anomalies, which then may cause suppressed precipitation in Southern Australia through the meridional advection of dry air from higher latitudes. However, this process may depend on the local wind anomalies in Australia, and the CESM may barely resolve this local process because of its lower horizontal resolution. As a result, the Australian precipitation anomalies in the CESM warm year composite exhibited diverse patterns in observations, the equatorial Pacific, and the Atlantic partial assimilation runs (upper panels in Figure 9).

Cold Composite of SLP and SST Anomalies

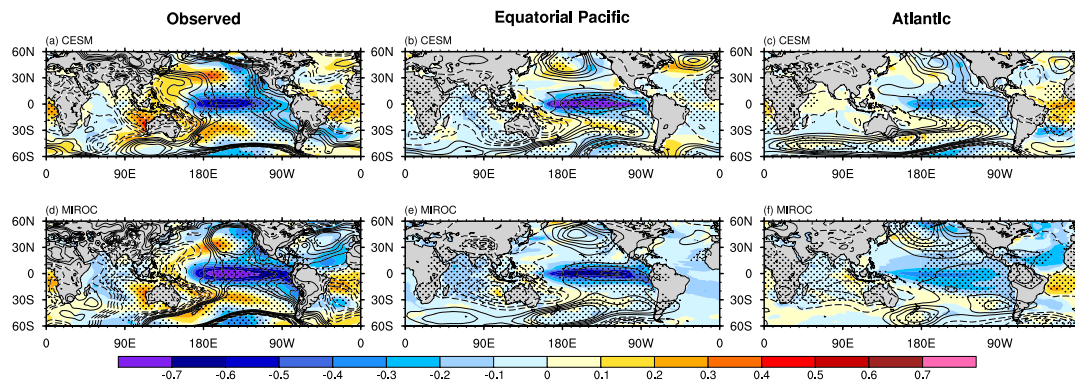


Figure 10. Annual mean SST (color interval is $0.1\text{ }^{\circ}\text{C}$) and SLP anomalies (contour interval is 0.2 hPa) in (a,d) observation, the (b,e) equatorial Pacific, and the (c,f) Atlantic partial assimilation runs during the cold year composites in the (top) CESM and the (bottom) MIROC. The dotted region is above the 90% significance level using Student's *t*-tests for SLP anomalies.

Warm Composite of SLP and SST Anomalies

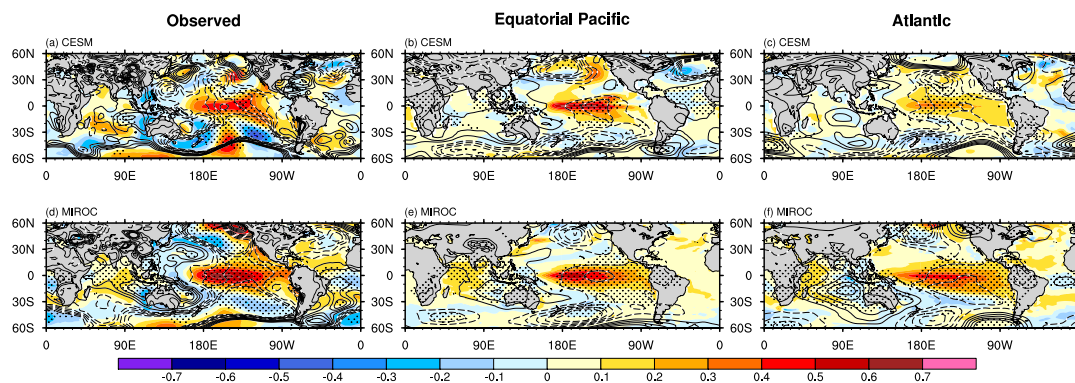


Figure 11. Annual mean SST (color interval is $0.1\text{ }^{\circ}\text{C}$) and SLP anomalies (contour interval is 0.2 hPa) in (a,d) observation, the (b,e) equatorial Pacific, and the (c,f) Atlantic partial assimilation runs during the warm year composites in the (top) CESM and the (bottom) MIROC. The dotted region is above the 90% significance level using Student's *t*-tests for SLP anomalies.

4. Discussion

Consistent with previous studies [24–27,29,52,60], our Atlantic partial assimilation runs identified the Atlantic's important impact on tropical Pacific climate variability through the tropical inter-basin gradients of SST and SLP anomalies between the Atlantic and the Pacific. In fact, our composite analyses of both observations and the Atlantic partial assimilation runs showed the tropical inter-basin contrast of SSTAs between the two oceans—the equatorial Pacific SST warming (cooling) was associated with the SST cooling (warming) in the Southern tropical Atlantic Ocean during the warm (cold) year composites in both the MIROC and CESM (left and right panels in Figures 10 and 11). During the cold year composites in particular, we found warm SST and negative SLP anomalies in the Southern tropical Atlantic in observations and the Atlantic partial assimilation runs (left and right panels in Figure 11), which consisted of the tropical inter-basin SST and SLP gradients. Notably, the equatorial Pacific partial assimilation runs showed unclear responses in the tropical Atlantic SSTAs (Figures 4d, 5d, 10b, 10e, 11b and 11e), supporting our hypothesis about the Atlantic origin of the tropical Pacific climate variability. Our findings are also consistent with previous studies, in which the Southern tropical Atlantic SST warming was shown to affect the inter-basin gradient of SLP anomalies, which triggers the central Pacific SST cooling through the modulation of global Walker

circulation [44]. Previous studies referred to the inter-basin SST and SLP gradients as the trans-basin variability (TBV) [25,29].

Based on the TBV perspective, our study implies the following process associated with Atlantic impacts on Australian precipitation variability. The SSTAs in the tropical Atlantic cause atmospheric vertical motions and its compensating vertical motions in the central tropical Pacific, which results in changes in the Pacific Walker circulation. Once the Pacific Walker circulation changes due to Atlantic forcings, it drives atmosphere–ocean interactions in the tropical Pacific through local Bjerknes feedback. Due to the fully coupled climate models, we identified a La Niña-like atmosphere–ocean response to the Atlantic forcing. However, it is still unclear what role the three-dimensional ocean field has on the low frequency ocean variability. Because Australia is located in the Western part of the Pacific Walker circulation, the vertical motion associated with the changes in the Western part of Pacific Walker circulation directly affects Australian precipitation variability. As a result, the warmer (colder) SSTAs in the tropical Atlantic cause SST cooling (warming) in the central Pacific, which, in turn, induces the upward (downward) motions and enhanced (suppressed) precipitation over Australia through the strengthened (weakened) Pacific Walker circulation. It is still unclear from this research which mechanisms regulate the warming or cooling of the Atlantic.

In addition to the Pacific and Atlantic basins, the Indian Ocean may also have a role in Australian precipitation variability. SST correlations associated with the first SVD modes showed a dipole-like pattern in the Indian Ocean—negative correlations in the west and positive in the east, except for the CESM Atlantic run (Figures 4a–e and 5a–f). These patterns resemble the IOD [16,17] and Ningaloo Niño [61], which are known to affect precipitation over Australia [13,62]. In addition to these impacts on Australian precipitation variability, the Indian Ocean could influence the Pacific Ocean through an atmospheric bridge on the interannual-to-decadal timescale [23,28,63,64]. Further analysis regarding the inter-basin interaction among three oceans would be beneficial to better understand and improve the Australian precipitation predictability on interannual-to-decadal timescales.

From this research, there are implications for increased predictability of Australian wet/dry conditions. Whereas the current seasonal prediction of Australian precipitation relies mainly on ENSO predictive skills, multi-year predictability for wet/dry conditions in Australia could be achieved by utilizing the TBV predictability [65]. Generally speaking, climate variability on larger spatial scales has longer predictability [66]. Because the inter-basin interactions, such as the TBV, show larger spatial scales than ENSO due to including the Atlantic Ocean, the Atlantic impacts on the Australian precipitation variability may have longer timescales compared to ENSO. In fact, some state-of-the-art climate prediction systems show multi-year predictive skills for TBV, which reflects much longer predictability than ENSO [29,30]. Moreover, the Atlantic partial assimilation runs showed decadal variability with peaks and ridges lasting several years, particularly after the mid-1980s (Figures 1i and 2i), and additionally, there was a decadal peak of spectral power for Australian precipitation variability, particularly in the MIROC (Figure 3). The longer predictability of Australian precipitation could translate into better assessment of climate risks for agriculture, water resources, and fire probability [40,52].

5. Conclusions

This research evaluated the potential interannual-to-decadal predictability of Australian precipitation using fully-coupled global climate models: the MIROC and the CESM. By assimilating the observed ocean temperature and salinity in the global, equatorial Pacific, and Atlantic Oceans with 10-member ensemble suites, we evaluated impact of the oceans on Australian precipitation variability. Past researchers have mainly focused on the roles of the Indian and Pacific basins in precipitation anomalies in Australia, particularly on seasonal-to-interannual timescales [67–72]. This research, however, took into consideration the effects of the Atlantic basin and inter-basin interactions on Australian precipitation variability on interannual-to-decadal timescales. Our study also discussed

the importance of inter-basin interactions in climate predictability, as described in the previous studies [24–27,29,60,73,74].

The results of this study show that the Australia precipitation variability is mostly attributed to global ocean variability. In particular, the equatorial Pacific SST variability is the main driver for the observed precipitation variability in Australia. Interestingly, however, we also identified the Atlantic Ocean impacts on Australian precipitation variability by affecting changes in the tropical Pacific climate through the TBV mechanism. Our SVD analysis in the Atlantic partial assimilation runs suggests that the predictability of Australian decadal precipitation anomalies would be enhanced by utilizing the multi-year predictive skills of TBV [29]. By combining our result with the seasonal forecast of ENSO, Australian climatologists may be able to provide more accurate forecasts of Australian wet/dry conditions on seasonal to decadal timescales. Future work should focus on additional experiments using different models and examining the role of TBV in past and future climates. There is also a need to determine which mechanisms affect the warming and cooling of the Atlantic Ocean because Atlantic changes are important for the Australian decadal precipitation variability through changes in the tropical Pacific climate.

Author Contributions: Conceptualization, Z.F.J., Y.C. and J.-J.L.; Methodology, Z.F.J., Y.C. and T.M.; Validation, Z.F.J., Y.C. and T.M.; Formal Analysis, Z.F.J.; Investigation, Z.F.J.; Data Curation, Y.C. and T.M.; Writing, Review & Editing, Z.F.J., Y.C. and J.-J.L.; Visualization, Z.F.J.; Supervision, Y.C.; Project Administration, Y.C.; Funding Acquisition, Y.C.

Funding: This research was supported by the Utah Agricultural Experiment Station, Utah State University, and approved as journal paper number 9109.

Acknowledgments: This manuscript benefited from the constructive comments of two anonymous reviewers. The CESM experiment in this paper was conducted by the University of Southern California Center for High-Performance Computing and Communications (<http://hpcc.usc.edu>) and the high-performance computing support from Yellowstone (ark:/85065/d7wd3xhc) provided by NCAR's Computational and Information Systems Laboratory sponsored by the National Science Foundation. The MIROC experiment was supported by the Japanese Ministry of Education, Culture, Sports, Science and Technology, through the Integrated Research Program for Advancing Climate Models. The simulations were performed with the Earth Simulator at the Japan Agency for Marine Earth Science and Technology. GPCC, ERSSTv4 and NCEP data sets are provided by the NOAA/OAR/ESRL PSD, Boulder, Colorado, USA, from their Web site at <http://www.esrl.noaa.gov/psd/>.

Conflicts of Interest: The founding sponsors had no role in the design of the study; in the collection, analyses, or interpretation of data; in the writing of the manuscript, and in the decision to publish the results.

Abbreviations

The following abbreviations are used in this manuscript:

ENSO	El Niño Southern Oscillation
IOD	Indian Ocean Dipole
TBV	Trans-basin variability
SLP	Sea level pressure
SST	Sea surface temperature
SSTA	Sea surface temperature anomalies
CESM	Community Earth System Model
MIROC	Model for Interdisciplinary Research on Climate
GPCC	Global Precipitation Climatology Centre
NCAR	National Center for Atmospheric Research
NCEP	National Centers for Environmental Prediction
SVD	Singular value decomposition

References

1. Heberger, M. Australia's millennium drought: Impacts and responses. In *The World's Water*; Springer: Heidelberg/Berlin, Germany, 2012; pp. 97–125.
2. Dijk, A.I.; Beck, H.E.; Crosbie, R.S.; Jeu, R.A.; Liu, Y.Y.; Podger, G.M.; Timbal, B.; Viney, N.R. The Millennium Drought in southeast Australia (2001–2009): Natural and human causes and implications for water resources, ecosystems, economy, and society. *Water Resour. Res.* **2013**, *49*, 1040–1057. [[CrossRef](#)]
3. Kiem, A.S.; Franks, S.W. Multi-decadal variability of drought risk, eastern Australia. *Hydrol. Processes* **2004**, *18*, 2039–2050. [[CrossRef](#)]
4. Horridge, M.; Madden, J.; Wittwer, G. The impact of the 2002–2003 drought on Australia. *J. Policy Model.* **2005**, *27*, 285–308. [[CrossRef](#)]
5. Yeo, S.W. Flooding in Australia: A review of events in 1998. *Nat. Hazards* **2002**, *25*, 177–191. [[CrossRef](#)]
6. Abrahams, M.; Price, J.; Whitlock, F.; Williams, G. The Brisbane floods, January 1974: Their impact on health. *Med. J. Aust.* **1976**, *2*, 936–939. [[PubMed](#)]
7. Chiew, F.H.; Piechota, T.C.; Dracup, J.A.; McMahon, T.A. El Nino/Southern Oscillation and Australian rainfall, streamflow and drought: Links and potential for forecasting. *J. Hydrol.* **1998**, *204*, 138–149. [[CrossRef](#)]
8. Philander, S.G.H. El Nino southern oscillation phenomena. *Nature* **1983**, *302*, 295. [[CrossRef](#)]
9. Allan, R.J. El Niño southern oscillation influences in the Australasian region. *Prog. Phys. Geogr.* **1988**, *12*, 313–348. [[CrossRef](#)]
10. Nicholls, N. The El Nino/southern oscillation and Australian vegetation. *Vegetatio* **1991**, *91*, 23–36. [[CrossRef](#)]
11. McDonald, J.; Drysdale, R.; Hill, D. The 2002–2003 El Nino recorded in Australian cave drip waters: Implications for reconstructing rainfall histories using stalagmites. *Geophys. Res. Lett.* **2004**, *31*. [[CrossRef](#)]
12. Bjerknes, J. Atmospheric teleconnections from the equatorial Pacific. *Mon. Weather Rev.* **1969**, *97*, 163–172. [[CrossRef](#)]
13. Ummenhofer, C.C.; England, M.H.; McIntosh, P.C.; Meyers, G.A.; Pook, M.J.; Risbey, J.S.; Gupta, A.S.; Taschetto, A.S. What causes southeast Australia's worst droughts? *Geophys. Res. Lett.* **2009**, *36*. [[CrossRef](#)]
14. Luo, J.J.; Masson, S.; Behera, S.K.; Yamagata, T. Extended ENSO predictions using a fully coupled ocean–atmosphere model. *J. Clim.* **2008**, *21*, 84–93. [[CrossRef](#)]
15. Meehl, G.A.; Goddard, L.; Boer, G.; Burgman, R.; Branstator, G.; Cassou, C.; Corti, S.; Danabasoglu, G.; Doblas-Reyes, F.; Hawkins, E.; et al. Decadal climate prediction: An update from the trenches. *Bull. Am. Meteorol. Soc.* **2014**, *95*, 243–267. [[CrossRef](#)]
16. Saji, N.; Goswami, B.; Vinayachandran, P.; Yamagata, T. A dipole mode in the tropical Indian Ocean. *Nature* **1999**, *401*, 360. [[CrossRef](#)] [[PubMed](#)]
17. Webster, P.J.; Moore, A.M.; Loschnigg, J.P.; Leben, R.R. Coupled ocean-atmosphere dynamics in the Indian Ocean during 1997–98. *Nature* **1999**, *401*, 356–360. [[CrossRef](#)] [[PubMed](#)]
18. Han, W.; Vialard, J.; McPhaden, M.J.; Lee, T.; Masumoto, Y.; Feng, M.; De Ruijter, W.P. Indian Ocean decadal variability: A review. *Bull. Am. Meteorol. Soc.* **2014**, *95*, 1679–1703. [[CrossRef](#)]
19. Wang, C. Atlantic climate variability and its associated atmospheric circulation cells. *J. Clim.* **2002**, *15*, 1516–1536. [[CrossRef](#)]
20. Luo, J.J.; Zhang, R.; Behera, S.K.; Masumoto, Y.; Jin, F.F.; Lukas, R.; Yamagata, T. Interaction between El Nino and extreme Indian ocean dipole. *J. Clim.* **2010**, *23*, 726–742. [[CrossRef](#)]
21. Luo, J.J.; Liu, G.; Hendon, H.; Alves, O.; Yamagata, T. Inter-basin sources for two-year predictability of the multi-year La Niña event in 2010–2012. *Sci. Rep.* **2017**, *7*, 2276. [[CrossRef](#)] [[PubMed](#)]
22. Rodríguez-Fonseca, B.; Polo, I.; García-Serrano, J.; Losada, T.; Mohino, E.; Mechoso, C.R.; Kucharski, F. Are Atlantic Niños enhancing Pacific ENSO events in recent decades? *Geophys. Res. Lett.* **2009**, *36*. [[CrossRef](#)]
23. Luo, J.J.; Sasaki, W.; Masumoto, Y. Indian Ocean warming modulates Pacific climate change. *Proc. Natl. Acad. Sci. USA* **2012**, *109*, 18701–18706. [[CrossRef](#)] [[PubMed](#)]
24. Chikamoto, Y.; Kimoto, M.; Watanabe, M.; Ishii, M.; Mochizuki, T. Relationship between the Pacific and Atlantic stepwise climate change during the 1990s. *Geophys. Res. Lett.* **2012**, *39*, L21710. [[CrossRef](#)]
25. McGregor, S.; Timmermann, A.; Stuecker, M.F.; England, M.H.; Merrifield, M.; Jin, F.F.; Chikamoto, Y. Recent Walker circulation strengthening and Pacific cooling amplified by Atlantic warming. *Nat. Clim. Chang.* **2014**, *4*, 888–892. [[CrossRef](#)]

26. Kucharski, F.; Ikram, F.; Molteni, F.; Farneti, R.; Kang, I.S.; No, H.H.; King, M.P.; Giuliani, G.; Mogensen, K. Atlantic forcing of Pacific decadal variability. *Clim. Dyn.* **2016**, *46*, 2337–2351. [[CrossRef](#)]
27. Li, X.; Xie, S.P.; Gille, S.T.; Yoo, C. Atlantic-induced pan-tropical climate change over the past three decades. *Nat. Clim. Chang.* **2015**. [[CrossRef](#)]
28. Izumo, T.; Vialard, J.; Lengaigne, M.; de Boyer Montegut, C.; Behera, S.K.; Luo, J.J.; Cravatte, S.; Masson, S.; Yamagata, T. Influence of the state of the Indian Ocean Dipole on the following year's El Niño. *Nat. Geosci.* **2010**, *3*, 168. [[CrossRef](#)]
29. Chikamoto, Y.; Timmermann, A.; Luo, J.J.; Mochizuki, T.; Kimoto, M.; Watanabe, M.; Ishii, M.; Xie, S.P.; Jin, F.F. Skillful multi-year predictions of tropical trans-basin climate variability. *Nat. Commun.* **2015**, *6*, 6869. [[CrossRef](#)] [[PubMed](#)]
30. Choudhury, D.; Gupta, A.S.; Sharma, A.; Taschetto, A.S.; Mehrotra, R.; Sivakumar, B. Impacts of the tropical trans-basin variability on Australian rainfall. *Clim. Dyn.* **2017**, *49*, 1617–1629. [[CrossRef](#)]
31. Power, S.; Tseitin, F.; Mehta, V.; Lavery, B.; Torok, S.; Holbrook, N. Decadal climate variability in Australia during the twentieth century. *Int. J. Climatol.* **1999**, *19*, 169–184. [[CrossRef](#)]
32. Becker, A.; Finger, P.; Meyer-Christoffer, A.; Rudolf, B.; Ziese, M. *GPCC Full Data Reanalysis Version 6.0 at 1.0: Monthly Land-Surface Precipitation From Rain-Gauges Built on GTS-Based and Historic Data*; Global Precipitation Climatology Centre (GPCC): Berlin, Germany, 2011.
33. Kalnay, E.; Kanamitsu, M.; Kistler, R.; Collins, W.; Deaven, D.; Gandin, L.; Iredell, M.; Saha, S.; White, G.; Woollen, J.; et al. The NCEP/NCAR 40-year reanalysis project. *Bull. Am. Meteorol. Soc.* **1996**, *77*, 437–471. [[CrossRef](#)]
34. Huang, B.; Banzon, V.F.; Freeman, E.; Lawrimore, J.; Liu, W.; Peterson, T.C.; Smith, T.M.; Thorne, P.W.; Woodruff, S.D.; Zhang, H.M. Extended reconstructed sea surface temperature version 4 (ERSST.v4). Part I: Upgrades and intercomparisons. *J. Clim.* **2015**, *28*, 911–930. [[CrossRef](#)]
35. Shields, C.A.; Bailey, D.A.; Danabasoglu, G.; Jochum, M.; Kiehl, J.T.; Levis, S.; Park, S. The low-resolution CCSM4. *J. Clim.* **2012**, *25*, 3993–4014. [[CrossRef](#)]
36. Nozawa, T.; Nagashima, T.; Ogura, T.; Yokohata, T.; Okada, N.; Shiogama, H. *Climate Change Simulations with a Coupled Ocean-Atmosphere GCM Called the Model for Interdisciplinary Research on Climate: MIROC*; Center for Global Environmental Research: Tsukuba, Japan, 2007.
37. Gent, P.R.; Danabasoglu, G.; Donner, L.J.; Holland, M.M.; Hunke, E.C.; Jayne, S.R.; Lawrence, D.M.; Neale, R.B.; Rasch, P.J.; Vertenstein, M.; et al. The community climate system model version 4. *J. Clim.* **2011**, *24*, 4973–4991. [[CrossRef](#)]
38. Neale, R.B.; Richter, J.; Park, S.; Lauritzen, P.H.; Vavrus, S.J.; Rasch, P.J.; Zhang, M. The mean climate of the Community Atmosphere Model (CAM4) in forced SST and fully coupled experiments. *J. Clim.* **2013**, *26*, 5150–5168. [[CrossRef](#)]
39. Lawrence, D.M.; Oleson, K.W.; Flanner, M.G.; Fletcher, C.G.; Lawrence, P.J.; Levis, S.; Swenson, S.C.; Bonan, G.B. The CCSM4 land simulation, 1850–2005: Assessment of surface climate and new capabilities. *J. Clim.* **2012**, *25*, 2240–2260. [[CrossRef](#)]
40. Chikamoto, Y.; Timmermann, A.; Stevenson, S.; DiNezio, P.; Langford, S. Decadal predictability of soil water, vegetation, and wildfire frequency over North America. *Clim. Dyn.* **2015**, *45*, 2213–2235. [[CrossRef](#)]
41. K-1 Model Developers. *K-1 Coupled GCM (MIROC) Description*; Center for Global Environmental Research: Tsukuba, Japan, 2004; Volume 1.
42. Komuro, Y.; Suzuki, T.; Sakamoto, T.T.; Hasumi, H.; Ishii, M.; Watanabe, M.; Nozawa, T.; Yokohata, T.; Nishimura, T.; Ogochi, K.; et al. Sea-ice in twentieth-century simulations by new MIROC coupled models: A comparison between models with high resolution and with ice thickness distribution. *J. Meteorol. Soc. Jpn.* **2012**, in press. [[CrossRef](#)]
43. Purich, A.; England, M.H.; Cai, W.; Chikamoto, Y.; Timmermann, A.; Fyfe, J.C.; Frankcombe, L.; Meehl, G.A.; Arblaster, J.M. Tropical Pacific SST drivers of recent Antarctic sea ice trends. *J. Clim.* **2016**, *29*, 8931–8948. [[CrossRef](#)]
44. Chikamoto, Y.; Mochizuki, T.; Timmermann, A.; Kimoto, M.; Watanabe, M. Potential tropical Atlantic impacts on Pacific decadal climate trends. *Geophys. Res. Lett.* **2016**, *43*, 7143–7151. [[CrossRef](#)]
45. Ham, Y.G.; Chikamoto, Y.; Kug, J.S.; Kimoto, M.; Mochizuki, T. Tropical Atlantic-Korea teleconnection pattern during boreal summer season. *Clim. Dyn.* **2017**, *49*, 2649–2664. [[CrossRef](#)]

46. Balmaseda, M.A.; Mogensen, K.; Weaver, A.T. Evaluation of the ECMWF ocean reanalysis system ORAS4. *Q. J. R. Meteorol. Soc.* **2013**, *139*, 1132–1161. [[CrossRef](#)]
47. Ishii, M.; Kimoto, M. Reevaluation of historical ocean heat content variations with time-varying XBT and MBT depth bias corrections. *J. Oceanogr.* **2009**, *65*, 287–299. [[CrossRef](#)]
48. Bloom, S.C.; Takacs, L.; da Silva, A.M.; Ledvina, D. Data assimilation using Incremental Analysis Updates. *Mon. Weather Rev.* **1996**, *124*, 1256–1271. [[CrossRef](#)]
49. Huang, B.; Kinter, J.; Schopf, P. Ocean data assimilation using intermittent analyses and continuous model error correction. *Adv. Atmos. Sci.* **2002**, *19*, 965–992. [[CrossRef](#)]
50. Mochizuki, T.; Ishii, M.; Kimoto, M.; Chikamoto, Y.; Watanabe, M.; Nozawa, T.; Sakamoto, T.T.; Shiogama, H.; Awaji, T.; Sugiura, N.; et al. Pacific Decadal Oscillation hindcasts relevant to near-term climate prediction. *Proc. Natl. Acad. Sci. USA* **2010**, *107*, 1833. [[CrossRef](#)] [[PubMed](#)]
51. Tatebe, H.; Ishii, M.; Mochizuki, T.; Chikamoto, Y.; Sakamoto, T.T.; Komuro, Y.; Mori, M.; Yasunaka, S.; Watanabe, M.; Ogochi, K.; et al. The initialization of the MIROC climate models with hydrographic data assimilation for decadal prediction. *J. Meteorol. Soc. Jpn.* **2012**, *90A*, 275–294. [[CrossRef](#)]
52. Chikamoto, Y.; Timmermann, A.; Widlansky, M.J.; Balmaseda, M.A.; Stott, L. Multi-year predictability of climate, drought, and wildfire in southwestern North America. *Sci. Rep.* **2017**, *7*, 6568. [[CrossRef](#)] [[PubMed](#)]
53. Zhang, R.; Delworth, T.L. Impact of the Atlantic multidecadal oscillation on North Pacific climate variability. *Geophys. Res. Lett.* **2007**, *34*, L23708. [[CrossRef](#)]
54. Kosaka, Y.; Xie, S.P. Recent global-warming hiatus tied to equatorial Pacific surface cooling. *Nature* **2013**, *501*, 403–407. [[CrossRef](#)] [[PubMed](#)]
55. Wallace, J.M.; Smith, C.; Bretherton, C.S. Singular Value Decomposition of Wintertime Sea Surface Temperature and 500-mb Height Anomalies. *J. Clim.* **1992**, *5*, 561–576. [[CrossRef](#)]
56. Van den Honert, R.C.; McAneney, J. The 2011 Brisbane floods: Causes, impacts and implications. *Water* **2011**, *3*, 1149–1173. [[CrossRef](#)]
57. Fensham, R. The influence of cattle grazing on tree mortality after drought in savanna woodland in north Queensland. *Aust. Ecol.* **1998**, *23*, 405–407. [[CrossRef](#)]
58. Trenberth, K.E. The definition of el nino. *Bull. Am. Meteorol. Soc.* **1997**, *78*, 2771–2777. [[CrossRef](#)]
59. Trenberth, K.E.; Stepaniak, D.P. Indices of el niño evolution. *J. Clim.* **2001**, *14*, 1697–1701. [[CrossRef](#)]
60. Kucharski, F.; Kang, I.; Farneti, R.; Feudale, L. Tropical Pacific response to 20th century Atlantic warming. *Geophys. Res. Lett.* **2011**, *38*, L03702. [[CrossRef](#)]
61. Feng, M.; McPhaden, M.J.; Xie, S.P.; Hafner, J. La Niña forces unprecedented Leeuwin Current warming in 2011. *Sci. Rep.* **2013**, *3*, 1277. [[CrossRef](#)] [[PubMed](#)]
62. Tozuka, T.; Kataoka, T.; Yamagata, T. Locally and remotely forced atmospheric circulation anomalies of Ningaloo Niño/Niña. *Clim. Dyn.* **2014**, *43*, 2197–2205. [[CrossRef](#)]
63. Han, W.; Meehl, G.A.; Hu, A.; Alexander, M.A.; Yamagata, T.; Yuan, D.; Ishii, M.; Pegion, P.; Zheng, J.; Hamlington, B.D.; et al. Intensification of decadal and multi-decadal sea level variability in the western tropical Pacific during recent decades. *Clim. Dyn.* **2014**, *43*, 1357–1379. [[CrossRef](#)]
64. Mochizuki, T.; Kimoto, M.; Watanabe, M.; Chikamoto, Y.; Ishii, M. Interbasin effects of the Indian Ocean on Pacific decadal climate change. *Geophys. Res. Lett.* **2016**, *43*, 7168–7175. [[CrossRef](#)]
65. Lee, J.Y.; Wang, B.; Kang, I.S.; Shukla, J.; Kumar, A.; Kug, J.S.; Schemm, J.; Luo, J.J.; Yamagata, T.; Fu, X.; et al. How are seasonal prediction skills related to models' performance on mean state and annual cycle? *Clim. dyn.* **2010**, *35*, 267–283. [[CrossRef](#)]
66. Baldwin, M.P.; Stephenson, D.B.; Thompson, D.W.; Dunkerton, T.J.; Charlton, A.J.; O'Neill, A. Stratospheric memory and skill of extended-range weather forecasts. *Science* **2003**, *301*, 636–640. [[CrossRef](#)] [[PubMed](#)]
67. Ropelewski, C.F.; Halpert, M.S. Global and Regional Scale Precipitation Patterns Associated with the El Niño/Southern Oscillation. *Mon. Weather Rev.* **1987**, *115*, 1606–1626. [[CrossRef](#)]
68. Meehl, G.A. The annual cycle and interannual variability in the tropical Pacific and Indian Ocean regions. *Mon. Weather Rev.* **1987**, *115*, 27–50. [[CrossRef](#)]
69. Dai, A.; Wigley, T.M.L. Global Patterns of ENSO-induced Precipitation 2000. *Geophys. Res. Lett.* **2000**, *27*, 1283–1286. [[CrossRef](#)]
70. Ashok, K.; Guan, Z.; Yamagata, T. Influence of the Indian Ocean Dipole on the Australian winter rainfall. *Geophys. Res. Lett.* **2003**, *30*. [[CrossRef](#)]

71. England, M.H.; Ummenhofer, C.C.; Santoso, A. Interannual rainfall extremes over southwest Western Australia linked to Indian Ocean climate variability. *J. Clim.* **2006**, *19*, 1948–1969. [[CrossRef](#)]
72. Ummenhofer, C.C.; Sen Gupta, A.; Briggs, P.R.; England, M.H.; McIntosh, P.C.; Meyers, G.A.; Pook, M.J.; Raupach, M.R.; Risbey, J.S. Indian and Pacific Ocean influences on southeast Australian drought and soil moisture. *J. Clim.* **2011**, *24*, 1313–1336. [[CrossRef](#)]
73. Timmermann, A.; Latif, M.; Voss, R.; Grötzner, A. Northern hemispheric interdecadal variability: A coupled air-sea mode. *J. Clim.* **1998**, *11*, 1906–1931. [[CrossRef](#)]
74. Okumura, Y.M.; Deser, C.; Hu, A.; Timmermann, A.; Xie, S.P. North Pacific climate response to freshwater forcing in the subarctic North Atlantic: Oceanic and atmospheric pathways. *J. Clim.* **2009**, *22*, 1424–1445. [[CrossRef](#)]



© 2018 by the authors. Licensee MDPI, Basel, Switzerland. This article is an open access article distributed under the terms and conditions of the Creative Commons Attribution (CC BY) license (<http://creativecommons.org/licenses/by/4.0/>).